

An improved arctangent algorithm based on phase-locked loop for heterodyne detection system

Chun-Hui Yan(晏春回), Ting-Feng Wang(王挺峰), Yuan-Yang Li(李远洋), Tao Lv(吕韬), Shi-Song Wu(吴世松)

Citation: Chin. Phys. B . 2019, 28(3): 030701. **doi:** 10.1088/1674-1056/28/3/030701
Journal homepage: http://cpb.iphy.ac.cn; http://iopscience.iop.org/cpb

What follows is a list of articles you may be interested in

Novel inspection of welded joint microstructure using magneto-optical imaging technology

Xiang-dong Gao(高向东), Zheng-wen Li(李正文), De-yong You(游德勇), Seiji Katayama

Chin. Phys. B . 2017, 26(5): 054214. **doi:** 10.1088/1674-1056/26/5/054214

Analysis of melt ejection during long pulsed laser drilling

Ting-Zhong Zhang(张廷忠), Zhi-Chao Jia(贾志超), Hai-Chao Cui(崔海超), De-Hua Zhu(朱德华), Xiao-Wu Ni(倪晓武), Jian Lu(陆健)

Chin. Phys. B . 2016, 25(5): 054206. **doi:** 10.1088/1674-1056/25/5/054206

Pump-induced carrier envelope offset frequency dynamics and stabilization of an Yb-doped fiber frequency comb

Zhao Jian, Li Wen-Xue, Yang Kang-Wen, Shen Xu-Ling, Bai Dong-Bi, Chen Xiu-Liang, Zeng He-Ping

Chin. Phys. B . 2014, 23(12): 124206. **doi:** 10.1088/1674-1056/23/12/124206

Chip design of a 5.8-GHz fractional-*N* frequency synthesizer with a tunable G_m–*C* loop filter

Huang Jhin-Fang, Liu Ron-Yi, Lai Wen-Cheng, Shin Chun-Wei, Hsu Chien-Ming

Chin. Phys. B . 2012, 21(8): 084210. **doi:** 10.1088/1674-1056/21/8/084210

A method of measuring micro-impulse with torsion pendulum based on multi-beam laser heterodyne

Li Yan-Chao,Wang Chun-Hui

Chin. Phys. B . 2012, 21(2): 020701. **doi:** 10.1088/1674-1056/21/2/020701

An improved arctangent algorithm based on phase-locked loop for heterodyne detection system*

Chun-Hui Yan(晏春回)[1,2], Ting-Feng Wang(王挺峰)[1,†], Yuan-Yang Li(李远洋)[1], Tao Lv(吕韬)[1,2], and Shi-Song Wu(吴世松)[1,2]

[1] State Key Laboratory of Laser Interaction with Matter, Changchun Institute of Optics, Fine Mechanics and Physics, Chinese Academy of Sciences, Changchun 130033, China
[2] University of Chinese Academy of Sciences, Beijing 100049, China

(Received 11 September 2018; revised manuscript received 27 December 2018; published online 23 January 2019)

We present an ameliorated arctangent algorithm based on phase-locked loop for digital Doppler signal processing, utilized within the heterodyne detection system. We define the error gain factor given by the approximation of Taylor expansion by means of a comparison of the measured values and true values. Exact expressions are derived for the amplitude error of two in-phase & quadrature signals and the frequency error of the acousto-optic modulator. Numerical simulation results and experimental results make it clear that the dynamic instability of the intermediate frequency signals leads to cumulative errors, which will spiral upward. An improved arctangent algorithm for the heterodyne detection is proposed to eliminate the cumulative errors and harmonic components. Depending on the narrow-band filter, our experiments were performed to realize the detectable displacement of 20 nm at a detection distance of 20 m. The aim of this paper is the demonstration of the optimized arctangent algorithm as a powerful approach to the demodulation algorithm, which will advance the signal-to-noise ratio and measurement accuracy of the heterodyne detection system.

Keywords: heterodyne detection, laser applications, arctangent algorithm, phase-locked loop

PACS: 07.60.Ly, 42.62.–b, 42.87.–d **DOI:** 10.1088/1674-1056/28/3/030701

1. Introduction

Optical heterodyne detection is a widely used interferometric technique measuring the phase of a temporal signal in the microwave region, which offers improved receiver sensitivity and better background noise rejection compared with the direct detection method.[1–5] This has been developed by researchers for many years. The heterodyne detection technique has good prospects of applications in micro-vibration and velocity measurements, rotation target spectrum identification, and laser ultrasonic propagation imager.

Based on the modulation phase of the photocurrent by the moving target, the frequency ω_1 of the measurement beam has to be mixed down by a reference beam from a coherent light source with frequency ω_2 in order to obtain the difference frequency relating to the heterodyne intermediate frequency signal, which carries the vibration information of the target. Usually, the reference beam is shifted in the frequency domain through an acousto-optic modulator whose driving signal is offered by a signal generator. Obviously, it is also possible to demodulate the phase of the intermediate frequency signal to acquire the instantaneous displacement information according to the relation with the phase and displacement of the Doppler signal.[6,7]

There are many demodulation algorithms in the heterodyne detection system, including the differential and cross-multiplying (DCM), the differential and self-multiplying (DSM), and the arctangent approach.[8–10] The former two algorithms are seriously affected by fluctuations of the light intensity due to the existence of differential calculation. The arctangent demodulation algorithm is common in the field of heterodyne detection, which has advantages of simplicity and high efficiency.

In addition, frequency and phase encoding techniques can be used in heterodyne systems to further improve the system performance.[11,12] Heterodyne systems are very sensitive to the phase fluctuation of the optical carrier and their performance can be seriously deteriorated in the presence of the higher carrier phase noise.[13–16] Subsequently, the displacement resolution and performance of the laser heterodyne detection system depend on not only the photodetector, laser source, and the matching process of signal light and local oscillator light but also the rest of the system, such as the acousto-optic modulator and the demodulation algorithm. If we want to investigate the long-range heterodyne detection, we also need to take the effects of atmospheric turbulence into consideration in addition. In our experiments, we perform a short-range heterodyne detection with the high-performance photodetector and laser source. Consequently, the accuracy of the acousto-optic modulator and the demodulation algorithm are dominant research components in this paper.

*Project supported by Key Research Program of Frontier Science, Chinese Academy of Sciences (Grant No. QYZDB-SSW-SLH014) and the Yong Scientists Fund of the National Natural Science Foundation of China (Grant No. 61205143).

†Corresponding author. E-mail: tingfeng_w@sina.com

© 2019 Chinese Physical Society and IOP Publishing Ltd

In Section 2, we introduce the process of the arctangent demodulation algorithm and establish a physical model between the measured values and true values of the phase of the intermediate frequency signal based on the error gain factor, which indicates the relations between the measured values and true values. The fluctuations of the phase cause the instability of the intermediate frequency signal, as reflected in higher harmonic components. Furthermore, the amplitude error of two in-phase (I) & quadrature (Q) signals can be effectively eliminated by the phase unwrapping process of the arctangent algorithm. Therefore the frequency error of an acousto-optic modulator has greater impacts on the demodulated results.

In Section 3, numerical results are presented to indicate that there are cumulative errors and higher harmonic components in the demodulation output in the absence and the presence of background noise. But the demodulation result is worse or even distorted in the noisy environment. An improved arctangent demodulation algorithm based on phase-locked loop gives outstanding performance to the heterodyne detection system. When the frequency of the target vibration is 1000 Hz, we set the bandwidth of the bandpass filer to 900–1100 Hz. Then the detectable displacement of the heterodyne detection system with the improved arctangent algorithm is approximately 20 nm at the detection distance of 30 m. It should be noted that narrowing the bandwidth of the bandpass filter is only suitable for a single frequency vibration not a complex vibration.

2. Theory

In general, the electrical field of the received light is frequency-modulated due to the target vibration. We can obtain the output photocurrents of the balanced detection[17,18]

$$i(t) = 2K\sqrt{P_{\rm s}(t)P_{\rm LO}(t)}\cdot\cos\left(\omega_{\rm s}t+\varphi_{\rm s}(t)-\varphi_{\rm LO}(t)\right), \quad (1)$$

where K is the conversion parameter, $K=\eta q/h\nu$, h is the Planck constant, ν is the optical frequency, η is the quantum efficiency, q is the charge of an electron. $P_{\rm LO}$ and $P_{\rm s}$ are the optical powers of the local oscillator beam and the measurement beam, respectively, $\omega_{\rm s}$ is the angular frequency of the intermediate frequency signal, and $\varphi_{\rm s}(t)$ and $\varphi_{\rm LO}(t)$ are the phase fluctuations of the signal beam and the local oscillator beam, respectively. The intermediate frequency signal consists of two components, the driving signal of an acousto-optic modulator and the Doppler signal generated by the moving target

$$\omega_{\rm s}t = 2\pi\left[f_{\rm AOM}+\frac{2v(t)}{\lambda}\right]t = 2\pi f_{\rm AOM}t+\frac{4\pi s(t)}{\lambda}, \quad (2)$$

where λ is the laser wavelength, $f_{\rm AOM}$ is the frequency of the acousto-optic modulator, and $s(t)$ is the target vibration signal that we try to acquire.

In Fig. 1, we show the arctangent demodulation algorithm process. From this figure, it is inferred that the arctangent demodulation algorithm is a good choice to complete a demodulation process between the reservation of the Doppler signal and the removal of the driving signal of the acousto-optic modulator. The key prerequisite of the arctangent algorithm is a signal pair comprising in-phase (I) and quadrature (Q) components, whose voltage amplitudes depend on the phase angle

$$\begin{aligned} u_{\rm i}(t) &= U_{\rm i}\sin\left(2\pi f_{\rm AOM}t\right), \\ u_{\rm q}(t) &= U_{\rm q}\cos\left(2\pi f_{\rm AOM}t\right). \end{aligned} \quad (3)$$

Such a signal combination is called an I&Q baseband signal, as there is no frequency offset present. In the baseband, a signal pair is needed to carry the complete Doppler information: whereas the absolute value of displacement s is represented by each component, its sign can only be recovered from both signals in combination. Unlike the carrier signal whose frequency is $f_{\rm AOM}$, the I&Q components are DC voltages in the case of a stationary target. This means that only the moving target produces a Doppler shift.

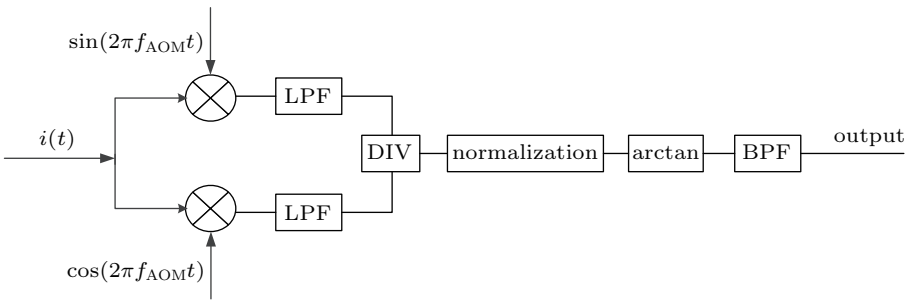


Fig. 1. The arctangent demodulation algorithm process, LPF: low-pass filter, DIV: division, BPF: bandpass filter.

In the process of quadrature demodulation, the differential current $i(t)$ is multiplied by sinusoidal and cosine carrier signals respectively. Through a low-pass filter, we can remove the sum-frequency components and retain the difference-frequency components

$$\begin{aligned} u_{\rm i}(t) &= \left|\left[i(t)\sin\left(2\pi f_{\rm AOM}t\right)\right]h_{\rm LPF}\right| \\ &= \frac{1}{2}K\sqrt{P_{\rm s}(t)P_{\rm LO}(t)}\sin\left(\frac{4\pi s(t)}{\lambda}+\varphi_{\rm s}(t)-\varphi_{\rm LO}(t)\right), \end{aligned}$$

$$u_{\mathrm{q}}(t) = |[i(t)\cos(2\pi f_{\mathrm{AOM}}t)]\,h_{\mathrm{LPF}}| = \frac{1}{2}K\sqrt{P_{\mathrm{s}}(t)P_{\mathrm{LO}}(t)}\cos\left(\frac{4\pi s(t)}{\lambda}+\varphi_{\mathrm{s}}(t)-\varphi_{\mathrm{LO}}(t)\right). \tag{4}$$

We order

$$\theta = 2\pi f_{\mathrm{AOM}}t, \quad \Delta\varphi = \frac{4\pi s(t)}{\lambda}+\varphi_{\mathrm{s}}(t)-\varphi_{\mathrm{LO}}(t). \tag{5}$$

In the ideal situation, the two signals have the same amplitude, no offset voltages are superimposed and the relative phase shift is exactly 90°. But in the actual situation, there is always a slight deviation because of the chip precision, the laser and acousto-optic modulator accuracies, or background noise.

Suppose voltages of two measured signals and actual frequencies of the acousto-optic modulator are respectively

$$\begin{cases} U_{\mathrm{i}} = U+\Delta U, \\ U_{\mathrm{q}} = U, \\ \theta_{\mathrm{i}} = \theta+\Delta\theta_{\mathrm{i}}, \\ \theta_{\mathrm{q}} = \theta+\Delta\theta_{\mathrm{q}}, \end{cases} \tag{6}$$

where U and θ represent the theoretical truth values, U_{i}, U_{q}, θ_{i}, and θ_{q} represent the actual measured values, ΔU, $\Delta\theta_{\mathrm{i}}$, and $\Delta\theta_{\mathrm{q}}$ represent the measurement errors. Then we can obtain

$$\tan\Delta\varphi = \frac{U+\Delta U}{U}\frac{\cos\Delta\theta_{\mathrm{i}}}{\cos\Delta\theta_{\mathrm{q}}}\tan\Delta\varphi_{\mathrm{m}}, \tag{7}$$

where $\Delta\varphi$ and $\Delta\varphi_{\mathrm{m}}$ indicate respectively the theoretical truth value and the actual demodulation measurement result, respectively. Now we define the error gain factor δ as

$$\delta = \frac{U+\Delta U}{U}\frac{\cos\Delta\theta_{\mathrm{i}}}{\cos\Delta\theta_{\mathrm{q}}}-1. \tag{8}$$

This becomes clear if equation (7) is written in the form of

$$\tan\Delta\varphi = (1+\delta)\tan\Delta\varphi_{\mathrm{m}}. \tag{9}$$

We find again

$$\Delta\varphi-\Delta\varphi_{\mathrm{m}} = \arctan\left[\frac{\delta\tan\varphi_{\mathrm{m}}}{1+(1+\delta)\tan^2\varphi_{\mathrm{m}}}\right] = f(\delta). \tag{10}$$

We know that $\Delta U/U$ is a very small value and $\cos\Delta\theta_{\mathrm{i}}$ is approximately equal to $\cos\Delta\theta_{\mathrm{q}}$, so δ is an infinitesimal. Then the function $f(\delta)$ has the following Taylor series expansion at $\delta = 0$:

$$f(\delta) = f(0)+f'(0)\delta+\frac{1}{2}f(0)''\delta^2+\frac{1}{6}f(0)'''\delta^3+o(\delta^3). \tag{11}$$

Noted that $o(\delta^3)$ is an infinitesimal of higher order. So we acquire the demodulation output result

$$\Delta\varphi \approx \Delta\varphi_{\mathrm{m}}+\frac{1}{2}\sin(2\Delta\varphi_{\mathrm{m}})\,\delta+\left[-\frac{1}{4}\sin(2\Delta\varphi_{\mathrm{m}})+\frac{1}{8}\sin(4\Delta\varphi_{\mathrm{m}})\right]\delta^2+\left[\frac{3}{12}\sin(2\Delta\varphi_{\mathrm{m}})-\frac{3}{12}\sin(4\Delta\varphi_{\mathrm{m}})+\frac{3}{24}\sin(6\Delta\varphi_{\mathrm{m}})\right]\delta^3+o(\delta^3). \tag{12}$$

As can be seen from Eq. (12), there is a small deviation of the higher harmonic components between the measured values and true values of the phase of the intermediate frequency signal. It is the fluctuations of the phase of the intermediate frequency signal that causes the instability of its frequency. Accordingly, we put forward an ameliorated arctangent algorithm based on phase-locked loop to track the frequency of the intermediate frequency signal.

As well we can obtain direct quantitative relationships between the amplitude error of two I&Q signals ΔU, the frequency error of the acousto-optic modulator $\Delta\theta$ and the error gain factor δ

$$\delta\big|_{\cos\Delta\theta_{\mathrm{i}}=\cos\Delta\theta_{\mathrm{q}}} = \Delta U/U, \quad \delta\big|_{\Delta U=0} = \frac{\cos\Delta\theta_{\mathrm{i}}}{\cos\Delta\theta_{\mathrm{q}}}-1 \approx \frac{1}{2}\left((\Delta\theta_{\mathrm{q}})^2-(\Delta\theta_{\mathrm{i}})^2\right). \tag{13}$$

It should be mentioned that equation (13) is an approximation with assumptions during the derivation of the equation. In reality, these two assumptions are difficult to achieve due to the presence of noise. However, we can still draw some useful information: the error gain factor is proportional to the square difference of the frequency error of the acousto-optic modulator but inversely proportional to the amplitude of the orthogonal signal.

3. Numerical and experimental results

3.1. Numerical results

As suggested in Section 2, the amplitude errors of two I&Q signals ΔU and the frequency errors of the acousto-optic modulator $\Delta\theta$ are important factors affecting the accuracy of demodulation outputs. In the simulation environment, we realize the whole process of the arctangent demodulation algorithm, which can achieve the demodulation output with the target vibration characteristics. Before the numerical simulations, we set some parameters globally: the frequency of the acousto-optic modulator $\omega_{\mathrm{s}} = 20$ MHz, the wavelength of the laser source $\lambda = 1550$ nm, the frequency of the target vibration $f_{\mathrm{s}} = 1000$ Hz, the target vibration amplitude $A_{\mathrm{s}} = 100$ nm. The numerical simulation results of the effects of ΔU and $\Delta\theta$ on demodulation outputs are evaluated with the following figures.

Figure 2 shows the variation of demodulation results with the frequency error of the acousto-optic modulator $\Delta\theta$ under the ideal environment. As can be seen from the five figures, no matter how small the frequency error is, there is always a cumulative error, and it increases with time. Although the cumulative error still exists when the accuracy is better to a certain extent, the demodulated results are not affected by the frequency error in a limited range. In other words, if we want better demodulated results, we should put forward higher requirements for the accuracy of the acousto-optic modulator.

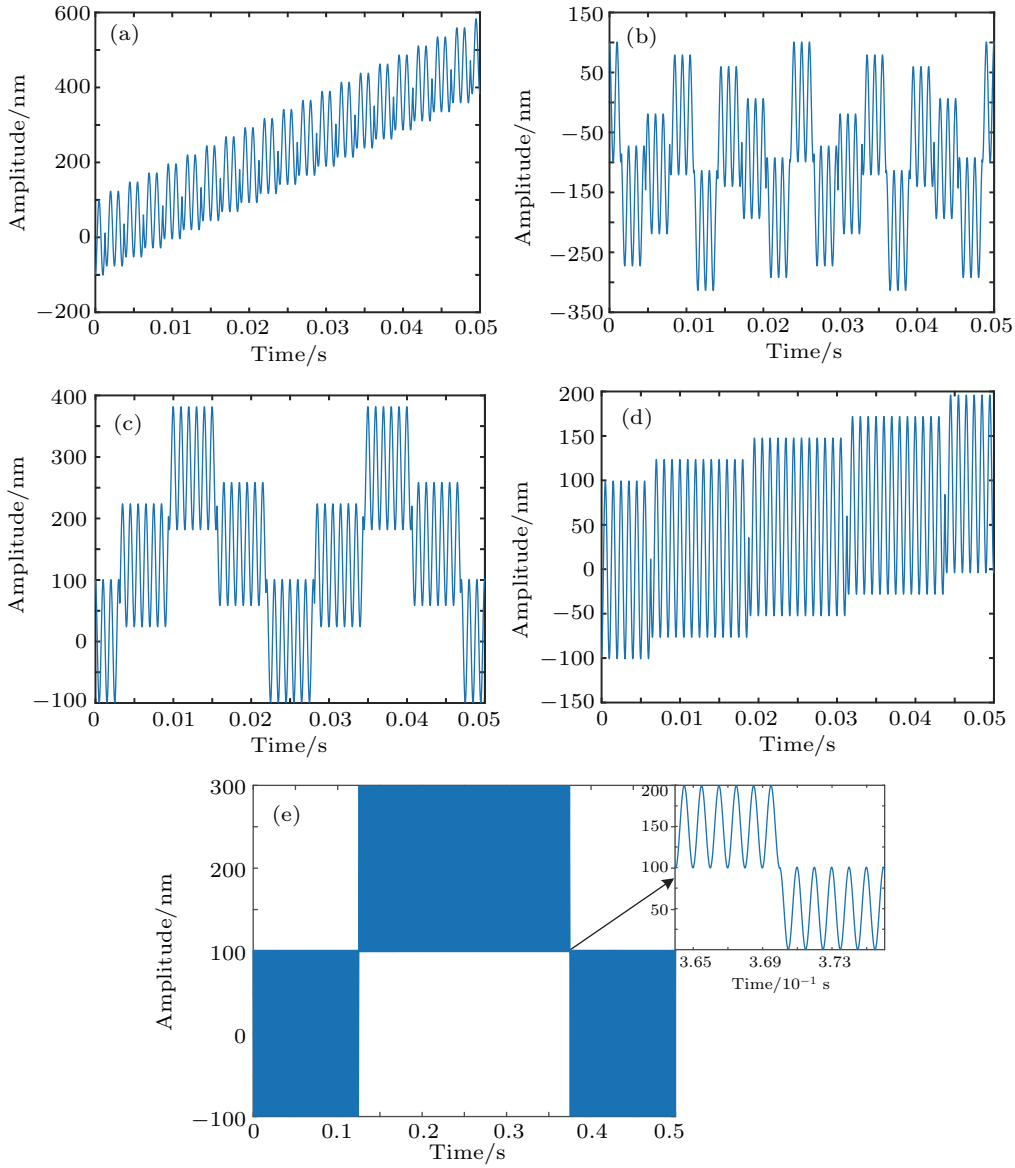


Fig. 2. Demodulation results varies with the frequency error of the acousto-optic modulator $\Delta\theta$; in panels (a)–(e), the accuracies of the acousto-optic modulators $\Delta\theta/\theta$ are 1×10^{-5}, 8×10^{-6}, 4×10^{-6}, 2×10^{-6}, and 1×10^{-7}, respectively.

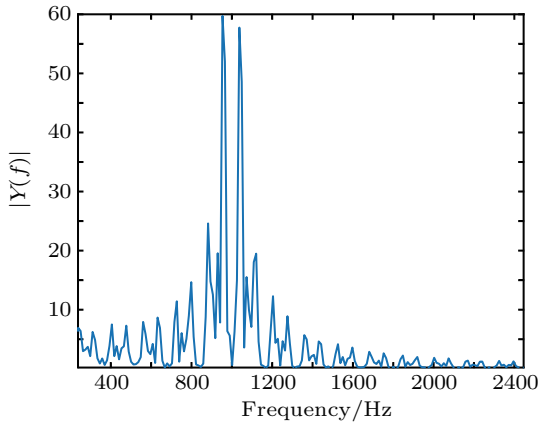


Fig. 3. The single amplitude spectrum of demodulated signal of the acousto-optic modulators.

Figure 3 shows the single amplitude spectrum of the demodulated signals with the accuracy of the acousto-optic modulator $\Delta\theta/\theta = 2\times10^{-6}$. It is evident that there are many harmonic components because of the frequency error of the acousto-optic modulator $\Delta\theta$. Thus a decrease of the accuracy of the acousto-optic modulator will lead to a reduction of the signal-to-noise ratio and displacement resolution of the system due to the instability of the intermediate frequency signal. A close agreement can be seen between the theoretical and numerical results. Then we will continue experimenting to verify the theoretical analyses.

Figure 4 illustrates the variation of demodulation results with the frequency error of the acousto-optic modulator $\Delta\theta$ under the uniform random noise environment and the accuracy of the acousto-optic modulator is 1×10^{-7}. In the simulation process, the uniform random noise is added to the carrier signal, and the ratios of the noise amplitude to the carrier signal are 0.1, 0.01, and 0.001, respectively. The demodulation deviation observed in this figure indicates that the demodulation result is worse even distorted when the noise reaches a certain

level. The cumulative error and the harmonic components still exist.

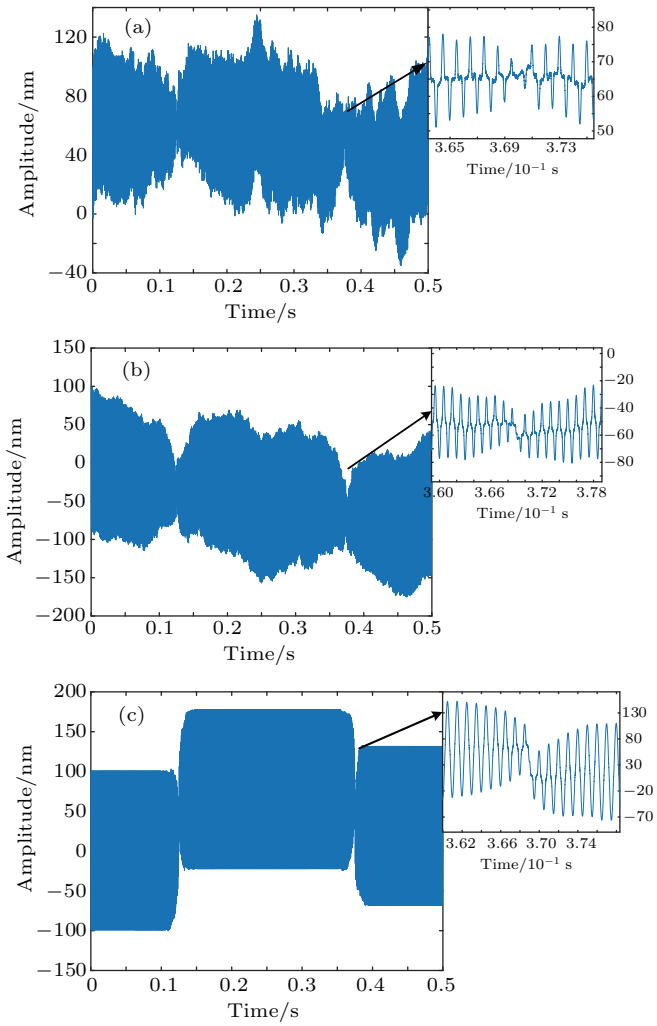


Fig. 4. Demodulation results vary with the frequency error of the acousto-optic modulator $\Delta\theta$ under noisy environment; in panels (a)–(c), the relative amplitude of noise is 0.1, 0.01, and 0.001, respectively.

From the principle of the arctangent demodulation algorithm, we know that the amplitude error of two I&Q signals will lead to a coefficient error in the demodulation result, which can be eliminated with the assistance of the phase unwrapping process of the arctangent demodulation algorithm. The numerical simulations also prove that the amplitude error of two I&Q signals has little effect on the demodulation results. However, the instability of the intermediate frequency (IF) signal will have a great influence on the demodulation result of the experiment. Then we will improve the experiment by adding a phase-locked loop (PLL) to track the IF signal frequency. If the frequency of the IF signal jitter is close to the frequency of the target vibration, it will be difficult for us to distinguish them by the filter. Fortunately, the frequency of the IF signal jitter is smaller than the target vibration frequency in practical engineering applications. Therefore this provides a possibility for us to track the frequency of the IF signal. Experiment results match the expectations and validate the feasibility of the improved algorithm.

3.2. Experimental results

The experiment setup is shown in Fig. 5 and a linearly polarized fiber laser with 10 kHz linewidth at the wavelength of 1.55 μm is selected as the light source.[19–21] In the process of laser transmission, we use polarization-maintaining fibers to maintain the direction of linear polarization and improve the signal-to-noise ratio of the coherent detection system, so as to achieve the high-precision measurement of target vibration characteristics. The frequency of the all-fiber acousto-optic modulator $f_{\mathrm{AOM}} = 20$ MHz. The balanced detection is an effective suppression of the local oscillator intensity noise in the heterodyne detection. However, dominant noise sources are not eliminated by means of the balanced detection and a careful matching of the carrier frequencies is necessary to avoid a severe system impairment. A standard 12-bit AD converter board digitizes output signals of the photodetector at a maximum sample rate of 200 Msa/s, which is sampled and processed the IF frequency signal with the phase-locked loop as shown in Fig. 6. And the arctangent algorithm based on the phase-locked loop is implemented in the hardware device.

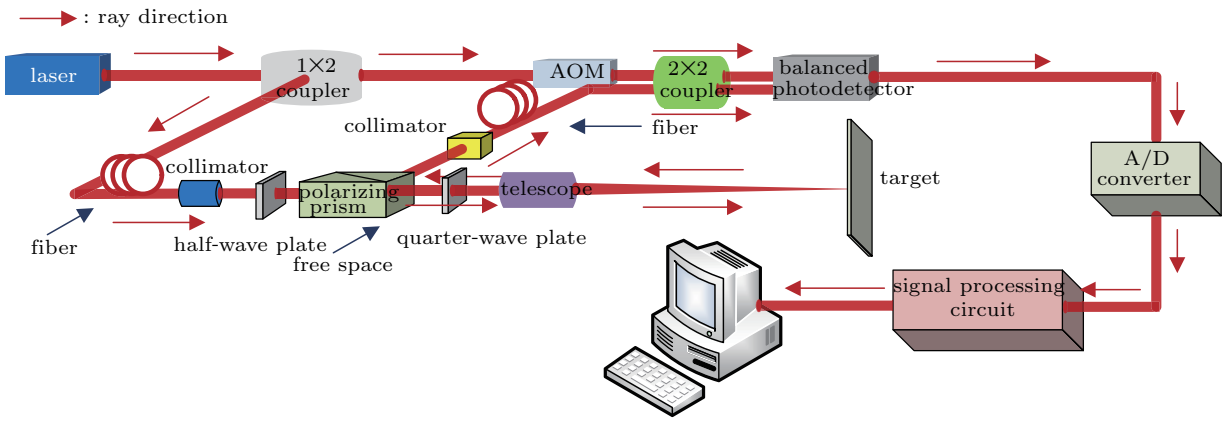


Fig. 5. The experimental setup of heterodyne detection system.

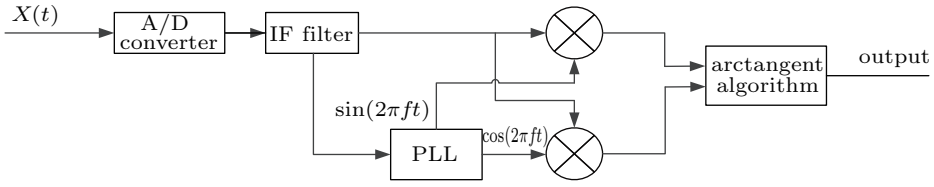


Fig. 6. The arctangent algorithm process based on PLL.

In this experiment, a linearly polarized beam with a wavelength of 1.55 μm is transmitted from a single-frequency continuous all-fiber laser. A 1 : 9 beam coupler divides the laser into two parts. The low power part serves as the local oscillator (LO) light and the other part serves as the signal light. The telescope transceiver system works as an interface between the signal light and echo signal reflected by the target. And the echo signal is mixed with the LO signal in a 3 dB coupler. Then the mixed signal detected by a balanced photodetector is known as the IF signal, whose frequency components include the driving frequency of the acousto-optic modulator and the Doppler frequency shift generated by the target modulation.

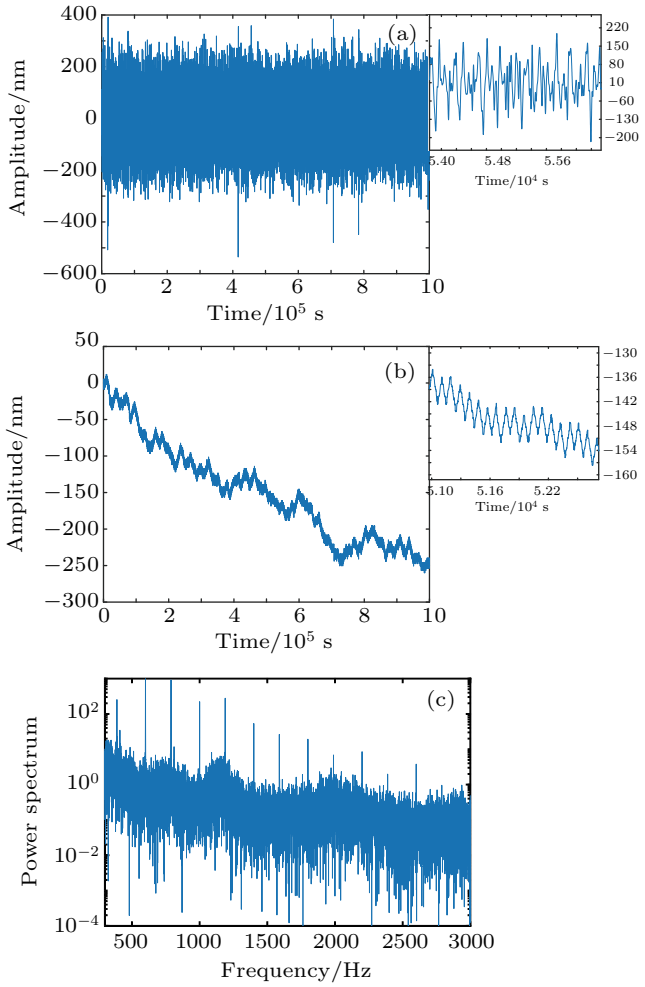


Fig. 7. (a), (b) The demodulation output results without PLL and (c) power spectrum when the signal to noise ratio is equal to −33.95 dB.

The signal generator generates sinusoidal waves with a frequency of 1000 Hz for the loudspeaker which drives the target to produce a standard sinusoidal vibration. The detection distance between the telescope and target is about 30 m and the vibration frequency of the target is 1000 Hz. A sinusoidal carrier signal at the frequency of 20 MHz is applied to the local oscillator light. Partial algorithm process and demodulation output results are implemented in the simulation software.

Figure 7 shows the demodulation output results of the target vibration without PLL. The demodulated signals are presented as amplitude graphs in Figs. 7(a) and 7(b). Figure 7(a) is processed by the bandpass filter, while figure 7(b) is not. Figure 7(c) shows the power spectrum of the demodulation results. The bandwidths of the bandpass filters in the experiment are 300–3000 Hz. According to the power spectrum, we calculate the SNR of the heterodyne detection system to be −33.95 dB. In the details of the demodulated signals shown in Fig. 7(b), it is obvious that there are cumulative errors and high-frequency noise components due to the instability of the IF signal and the demodulated waveform is irregular. This phenomenon is in accordance with the simulation result shown in Fig. 4.

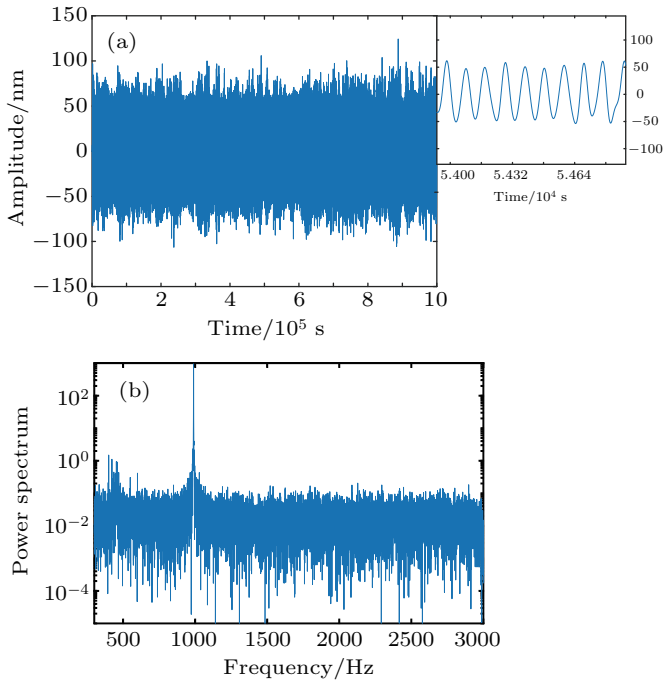


Fig. 8. (a) The demodulation output results with PLL and (b) power spectrum when the signal to noise ratio is equal to 14.69 dB.

Figure 8 shows the demodulation output results with PLL.

Figure 8(a) is the demodulation output result of the target vibration and figure 8(b) is the power spectrum of the output results. In this case, the SNR of the heterodyne detection system is equal to 14.69 dB and the output waveform is closer to the sine wave. The arctangent algorithm based on PLL is an efficient way to eliminate redundant harmonic components and improve the displacement resolution of the heterodyne detection system. Therefore, we believe that improving the stability of the IF signal can increase the signal-to-noise ratio of the heterodyne detection system.

For better measurement results shown in Fig. 9, the detectable displacement at a distance of 30 m of the heterodyne detection system is approximately 20 nm. Figures 9(b) and 9(d) show the partial enlarged details of Figs. 9(a) and 9(c). The bandwidth of the bandpass filer in Fig. 9(a) is still 300–3000 Hz but we set the bandwidth of the bandpass filer in Fig. 9(b) to 900–1100 Hz. In the target a sinusoidal vibration with a vibration frequency of 1000 Hz occurs. When the recovered vibration is also a standard sinusoidal vibration, we believe that the amplitude of the vibration is the detectable displacement of the heterodyne detection system. The demodulation result of Fig. 9(d) is close to the standard sinusoidal waveform. From Figs. 9(b) and 9(d), it can be deduced that the detectable displacement in Fig. 9(d) is approximately 20 nm. It should be noted that this method is only suitable for single frequency vibrations but not suitable for complex vibrations. So we can set different filter ranges to adapt different application scenarios.

It should be noted that there are many factors that affect the resolution of displacement. Firstly, standard sinusoidal micro-vibration detection brings a higher requirement for the target material and elastic deformation of the target may be distorted when the vibration amplitude is very small. Secondly, there are additional spurious noise components in heterodyne detection, which may push the practical limits of displacement resolution to lower level. As mentioned, the high resolution is feasible only under the provision of sufficiently small filter bandwidth of the subsequent signal processing system.

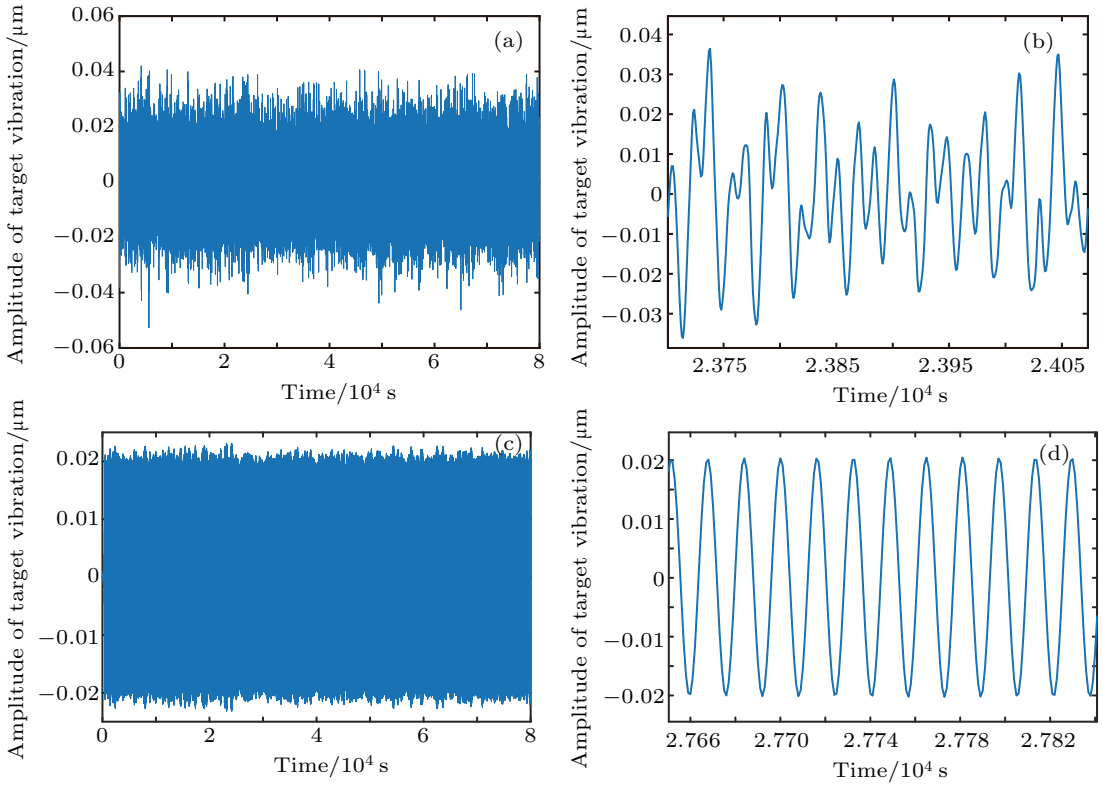


Fig. 9. The detectable displacement of target vibration when the detection distance is 30 m. In panels (a) and (c), the bandwidth of the bandpass filer is 300–3000 Hz and 900–1100 Hz, respectively; panels (b) and (d) are the corresponding partial enlarged details of panels (a) and (c).

4. Conclusion

We put forward an improved arctangent algorithm based on phase-locked loop in the field of heterodyne detection, which can improve the signal-to-noise ratio and detection accuracy of the system. The influence of amplitude errors of two I&Q signals and frequency errors of an acousto-optic modulator on the heterodyne detection is analyzed by theoretical derivations. According to the definition of the error gain factor, we have given the comparison between the measured values and true values of the phase of the IF signal. We set up an experiment to verify the feasibility and stability of the improved algorithm. The experimental results show that the instability of the intermediate frequency signal can be elimi-

nated and the cumulative error will disappear. The theoretical simulations and experimental results exhibit a good agreement during the research. Meanwhile, the ameliorated arctangent algorithm can improve the SNR of the heterodyne detection system. Our experimental setup has a detectable displacement of about 20 nm at a detection distance of 30 m.

References

[1] Deferrari H A, Darby R A and Andrews F A 1967 *J. Acoust. Soc. Am.* **42** 982

[2] Deferrari H A, Darby R A and Andrews F A 1968 *J. Acoust. Soc. Am.* **43** 1463

[3] Eberhardt F J and Andrews F A 1970 *J. Acoust. Soc. Am.* **47** 116

[4] Yu X C, Zhi Y, Tang S J, Li B B, Gong Q, Qiu C W and Xiao Y F 2018 *Light Sci. & Appl.* **7** 18003

[5] Traverso A J, O'Brien C, Hokr B H, Thompson J V, Yuan L, Ballmann C W, Svidzinsky A A, Petrov G I, Scully M O and Yakovlev V V 2016 *Light Sci. & Appl.* **6** e16262

[6] Saito S, Yamamoto Y and Kimura T 1980 *Electron. Lett.* **16** 826

[7] Bauer M, Ritter F and Siegmund G 2002 *Fifth International Conference on Vibration Measurements by Laser Techniques: Advances and Applications*, May 22–25, 2002 Ancona, Italy, p. 50

[8] He J, Wang L, Li F and Liu Y 2010 *J. Lightwave Technol.* **28** 3258

[9] Wang G, Xu T and Li F 2012 *OFS*2012 22*nd International Conference on Optical Fiber Sensors*, November 7–10, 2012, Beijing, China, p. 84219W-1

[10] Wu B, Yuan Y, Yang J, Liang S and Yuan L 2015 *Fifth Asia Pacific Optical Sensors Conference*, July 1–4, 2015, Jeju, Korea, p. 96550C

[11] Teich M C 2005 *Proc. IEEE* **56** 37

[12] Jakeman E, Oliver C J and Pike E R 1971 *Phys. Lett. A* **34** 101

[13] Watanabe S, Naito T, Chikama T and Kuwahara H 2002 *J. Lightwave Technol.* **10** 1963

[14] Wang B, Fan X, Wang S, Yang G, Liu Q and He Z 2016 *Opt. Commun.* **365** 220

[15] Venkatesh S and Sorin W V 1993 *J. Lightwave Technol.* **11** 1694

[16] Armstrong J A 1966 *J. Opt. Soc. Am.* **56** 1024

[17] Painchaud Y, Poulin M, Morin M and Têtu M 2009 *Opt. Express* **17** 3659

[18] Stierlin R, Bättig R, Henchoz P D and Weber H P 1986 *Opt. & Quantum Electron.* **18** 445

[19] Matson C L 1998 *Proc. SPIE - Int. Soc. For Opt. Eng.* **3380** 243

[20] Fang F, Zhang Y, Zhou D and Zhang G 1996 *Automated Optical Inspection for Industry*, October 3–6, 2012, Beijing, China, p. 599

[21] Permeneva D 2014 *Optical Heterodyne Detection of Phase-Shifted Signals* (MS Dissertation) (New York: Rochester Institute of Technology)